PLOS ONE

RESEARCH ARTICLE

The Influence of the 1-(3-Trifluoromethyl-Benzyl)-1*H*-Pyrazole-4-yl Moiety on the Adenosine Receptors Affinity Profile of Pyrazolo[4,3-*e*][1,2,4]Triazolo[1,5-*c*] Pyrimidine Derivatives

Stephanie Federico[1]*, Sara Redenti[1], Mattia Sturlese[2], Antonella Ciancetta[2], Sonja Kachler[3], Karl-Norbert Klotz[3], Barbara Cacciari[4], Stefano Moro[2], Giampiero Spalluto[1]*

1 Dipartimento di Scienze Chimiche e Farmaceutiche, Università degli Studi di Trieste, Trieste, Italy, **2** Molecular Modeling Section (MMS), Dipartimento di Scienze del Farmaco, Università degli Studi di Padova, Padova, Italy, **3** Institut für Pharmakologie und Toxicologie, Universität Würzburg, Würzburg, Germany, **4** Dipartimento di Scienze Chimiche e Farmaceutiche, Università degli Studi di Ferrara, Ferrara, Italy

* sfederico@units.it (SF); spalluto@units.it (GS)

Citation: Federico S, Redenti S, Sturlese M, Ciancetta A, Kachler S, Klotz K-N, et al. (2015) The Influence of the 1-(3-Trifluoromethyl-Benzyl)-1*H*-Pyrazole-4-yl Moiety on the Adenosine Receptors Affinity Profile of Pyrazolo[4,3-*e*][1,2,4]Triazolo[1,5-*c*] Pyrimidine Derivatives. PLoS ONE 10(12): e0143504. doi:10.1371/journal.pone.0143504

Editor: James Porter, University of North Dakota, UNITED STATES

Received: June 11, 2015

Accepted: November 5, 2015

Published: December 1, 2015

Data Availability Statement: All relevant data are within the paper and its Supporting Information files.

Funding: This work was supported by: Italian Ministry for University and Research, PRIN2008: protocol number 200834TC4L_002 (SM) and protocol number 200834TC4L_004 (GS SF); http://prin.miur.it/index.php?pag=2008. The funders had no role in study design, data collection and analysis, decision to publish, or preparation of the manuscript.

Abstract

A new series of pyrazolo[4,3-*e*][1,2,4]triazolo[1,5-*c*]pyrimidine (PTP) derivatives has been developed in order to explore their affinity and selectivity profile at the four adenosine receptor subtypes. In particular, the PTP scaffold was conjugated at the C2 position with the 1-(3-trifluoromethyl-benzyl)-1*H*-pyrazole, a group believed to confer potency and selectivity toward the human (h) A_{2B} adenosine receptor (AR) to the xanthine ligand 8-(1-(3-(trifluoromethyl)benzyl)-1*H*-pyrazol-4-yl)-1,3-dimethyl-1*H*-purine-2,6(3*H*,7*H*)-dione (CVT 6975). Interestingly, the synthesized compounds turned out to be inactive at the hA_{2B} AR but they displayed affinity at the hA_3 AR in the nanomolar range. The best compound of the series (**6**) shows both high affinity (hA_3 AR K_i = 11 nM) and selectivity (A_1/A_3 and A_{2A}/A_3 > 9090; A_{2B}/A_3 > 909) at the hA_3 AR. To better rationalize these results, a molecular docking study on the four AR subtypes was performed for all the synthesized compounds. In addition, CTV 6975 and two close analogues have been subjected to the same molecular docking protocol to investigate the role of the 1-(3-trifluoromethyl-benzyl)-1*H*-pyrazole on the binding at the four ARs.

Introduction

Adenosine is an ubiquitous modulator, which exerts its functions through interaction with four G protein-coupled receptors classified as A_1, A_{2A}, A_{2B} and A_3 adenosine receptors (ARs). [1,2] While A_1, A_{2A} and A_3 ARs are stimulated by low concentrations of adenosine, the A_{2B}

Competing Interests: SM participates in the European COST Action CM1207 (GLISTEN).

subtype requires higher concentrations of the natural ligand. [3] In recent years, numerous potent and selective ligands (agonists and antagonists) for the A_1, A_{2A}, A_{2B} and A_3 AR subtypes have been discovered. [4,5] Some of them served as pharmacological tools and demonstrated potential therapeutic applications in various pathological processes. For example, human (h) A_1 AR agonists are useful against cardiac arrhythmias and pain, while antagonists are beneficial in kidney failure. Antagonists for the hA_{2A} AR were widely studied for the treatment of Parkinson's disease and other neurodegenerative disorders. [3–5] To date, the physio-pathological role of the hA_3 AR is controversial. This AR subtype is involved in cancer and inflammation, although it is not yet clear whether blocking or activating this receptor would be therapeutic for these conditions. [6] Identification of potent and selective ligands for the hA_{2B} AR is difficult as compared with the other receptor subtypes. In addition, its characterization as a low-affinity adenosine receptor led to the erroneous belief that the A_{2B} AR was not of substantial physiological relevance. [7–9] As a consequence, the hA_{2B} AR is the least characterized among the ARs, although in the last years, significant advances have been made in the understanding of the molecular pharmacology and physiology of the hA_{2B} ARs. [7–9] This subtype is highly expressed during inflammatory and hypoxic conditions and, in these circumstances, adenosine reaches very high extracellular concentrations necessary to activate the hA_{2B} AR subtype. [9] In fact, the hA_{2B} ARs seem to be implicated in many different patho-physiological conditions such as: asthma, [10–14] intestinal functions, vascular tone and permeability, ischemic preconditioning, inflammation, angiogenesis and sickle disease. [9,15–20] Therefore, hA_{2B} AR antagonists have been proposed as anti-asthmatic and/or anti-inflammatory agents. [4,5] In particular, most of the so far developed hA_{2B} AR antagonists are xanthine derivatives or analogues. [21] In 2006 a very interesting compound named CVT 6975 (8-(1-(3-(trifluoromethyl) benzyl)-1*H*-pyrazol-4-yl)-1,3-dimethyl-1*H*-purine-2,6(3*H*,7*H*)-dione (**1**, Fig 1) proved to be one of the most potent A_{2B} AR antagonists ever reported. [22] In the non-xanthine family, some adenine [23], 7-deazapurines [24], triazolo-triazine, [24] quinazoline, [25], triazinobenzimidazole [26], pyrimidine [27] and pyrazine [28] derivatives have been reported as hA_{2B} AR antagonists, but few of the synthesized compounds (e.g. pyrimidines) showed both significant potency and selectivity for this receptor subtype.

In one of our research programs aimed at the identification of new non-xanthine hA_{2B} AR antagonists, we investigated variously substituted pyrazolo[4,3-*e*][1,2,4]triazolo[1,5-*c*]pyrimidine (PTP) derivatives. [29–31] A large number of derivatives with different substitutions at the N7, N8 and N5 positions (see Fig 2 for numbering of the PTP ring system) have been prepared, but unfortunately none of the synthesized compounds showed both affinity and selectivity at the hA_{2B} ARs. [29–31] One of the most interesting compounds developed is derivative **2** (Fig 1), which displays good affinity for the hA_{2B} AR (K_i = 165 nM) but it shows a greater affinity towards the hA_3 AR (K_i = 0.81 nM). [32] Taking into account these experimental observations, we decided to synthesize new derivatives by replacing the furan moiety in position C2 of the PTP scaffold with the 1-(3-trifluoromethyl-benzyl)-1*H*-pyrazole-4-yl moiety present in the CVT 6975 (**1**) with the aim to better explore the role of this position in the receptor recognition and possibly obtain new A_{2B} AR antagonists with non xanthinic structure (Fig 2).

Materials and Methods

Chemistry

General. Reactions were routinely monitored by thin-layer chromatography (TLC) on silica gel (precoated F254 Merck plates). Flash chromatography was performed using Merck 60–200 mesh silica gel. Infrared spectra (IR) were measured on a Perkin Elmer 257 instrument. ^{1}H-NMR were determined in $CDCl_3$ or DMSO-d_6 solutions with a Varian Gemini 200

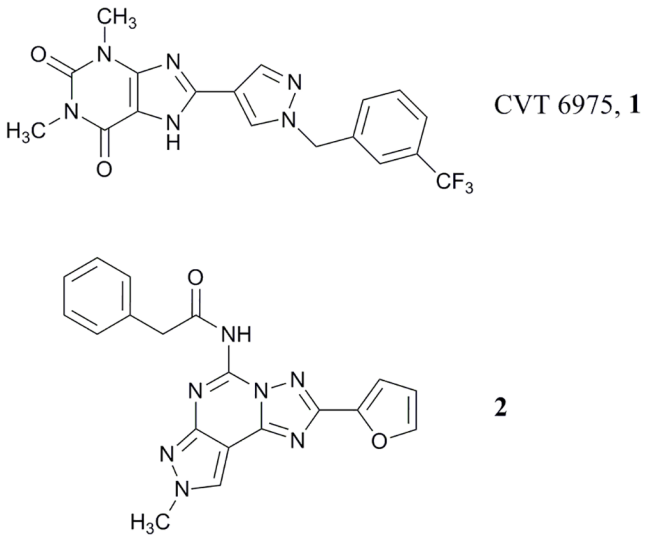

Fig 1. CVT6975 (1) and the pyrazolo[4,3-*e*][1,2,4]triazolo[1,5-*c*]pyrimidine derivative 2 as potent A_{2B} and A_3 AR antagonists, respectively.

doi:10.1371/journal.pone.0143504.g001

spectrometer, peaks positions are given in parts per million (δ) downfield relative to the central peak of the solvent; J values are given in Hz. Melting points were determined on a Buchi-Tottoli instrument and are uncorrected. All reported products showed IR and ^{1}H NMR spectra in agreement with the assigned structures. Electrospray mass spectra were recorded on a ESI

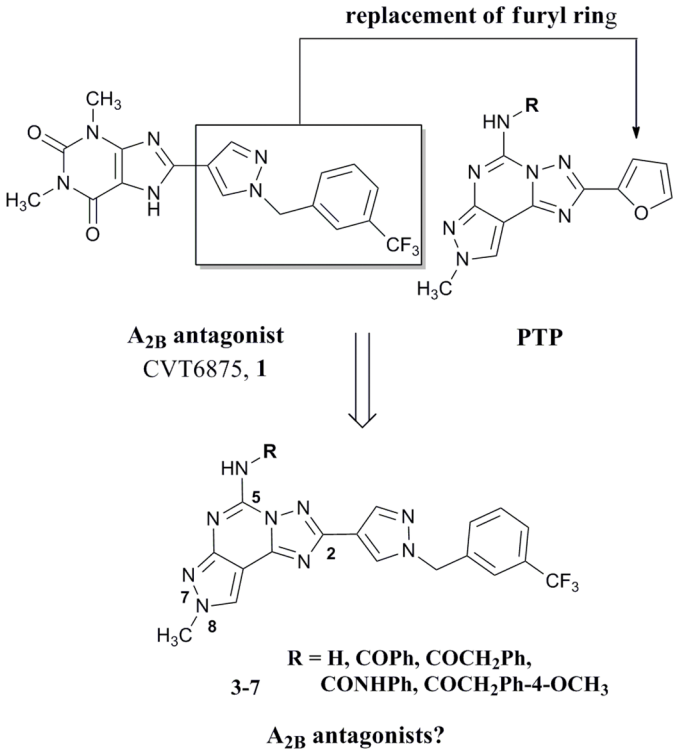

Fig 2. Rational for the design of the target compounds 3–7.

doi:10.1371/journal.pone.0143504.g002

Bruker 4000 Esquire spectrometer and compounds were dissolved in methanol. Elemental analyses were performed by the microanalytical laboratory of Dipartimento di Scienze Chimiche e Farmaceutiche, University of Trieste, and they were within ±0.4% of the theoretical values for C, H and N. Light petroleum ether refers to the fractions boiling at 40–60°C. Organic solutions were dried over anhydrous magnesium sulfate.

Synthesis of 1-(3-trifluoromethyl-benzyl)-1*H*-pyrazole-4-carboxylic acid hydrazide (10). Pyrazole ester derivative **9** (5.7 g, 20 mmol) was dissolved in absolute ethanol (30 mL) and an equivalent amount of hydrazine monohydrate (0.96 mL, 20 mmol) was added and the resulting mixture was stirred at reflux for three days. The solvent was then removed in vacuo and the residue crystallized from EtOAc to afford the corresponding hydrazide **9** as a white solid (mp 95°C) in quantitative yield. IR (KBr): 3445–2960, 1690, 1650, 1610, 1480 cm^{-1}; ^1H NMR ($CDCl_3$) δ: 3.65 (bs, 2H); 5.21 (s, 2H); 6.51 (bs, 1H); 7.21–7.58 (m, 4H); 7.66 (s, 1H); 7.77 (s, 1H). Anal. Calcd. for $C_{12}H_{11}N_4OF_3$ (MW 284.24): C, 50.71; H, 3.90; N, 19.17. Found: C, 50.53; H, 3.85; N, 19.18.

Synthesis of 8-methyl-2-[1-(3-trifluoromethyl-benzyl)-1*H*-pyrazol-4-yl]-8*H*-pyrazolo [4,3-*e*][1,2,4]triazolo[1,5-*c*]pyrimidin-5-ylamine (3). Pyrazole **8** (2.4 g, 20 mmol) was dissolved in diphenyl ether (30 mL) and hydrazide **10** (6.25 g, 22 mmol, 1.1 eq) was added. The mixture was heated at 260°C using a Dean-Stark for the azeotropic elimination of water produced in the reaction. After 2.5 h, the mixture was poured onto hexane (200 mL) and cooled. The precipitate of crude pyrazole-triazole derivative **11** was filtered off, and utilized for the next step without further purifications. The crude residue, was dissolved in N-methyl pyrrolidone (40 mL), cyanamide (3 eq, 60 mmol, 2.5 g) and *p*-toluen sulfonic acid (1.5 eq, 30 mmol, 5.7 g) were added and the mixture was heated at 160°C for 4 h. Cyanamide (3 eq, 60 mmol, 2.5 g) was added again and the solution was heated overnight. Then the solution was diluted with EtOAc (80 mL) and the precipitate (excess of cyanamide) was filtered off; the filtrate was concentrated under reduced pressure and washed with water (3 x 30 mL). The organic layer was dried (Na_2SO_4) and evaporated under vacuum. The residue was purified by flash chromatography (EtOAc/Methanol 9.5:0.5) to afford the desired compound **3** in a good overall yield (60%) as a yellow solid. Mp 125°C (EtOAc-light petroleum); IR (KBr): 3330–2960, 1640, 1605, 1550, 1450 cm^{-1}; ^1H NMR (DMSO-d_6) δ: 3.87 (s, 3H); 5.20 (s, 2H); 5.72 (bs, 2H); 7.18–7.41 (m, 4H); 7.84 (s, 1H); 7.96 (s, 1H); 7.97 (s, 1H). ES-MS: (MH^+) 414.4. Anal. Calcd. for $C_{18}H_{14}N_9F_3$ (MW 413.36): C, 52.30; H, 3.41; N, 30.50. Found: C, 52.13; H, 3.44; N, 30.38.

Synthesis of 1-{8-Methyl-2-[1-(3-trifluoromethyl-benzyl)-1*H*-pyrazol-4-yl]-8*H*-pyrazolo [4,3-*e*][1,2,4]triazolo [1,5-*c*]pyrimidin-5-yl}-3-phenylurea (4). Amino compound (**3**) (206 mg, 0.5 mmol) was dissolved in freshly distilled dioxane (15 mL) and phenyl isocyanate (130 μL, 1 mmol, 2 eq) was added. The mixture was refluxed under argon for 18 hours. Then the solvent was removed under reduced pressure and the residue was purified by flash chromatography (EtOAc-light petroleum 8:2) to afford the desired compound **4** in a good yield (88%) as a white solid, mp 180°C (EtOAc-light petroleum); IR (KBr): 3355–2980, 1705, 1655, 1600, 1530 cm^{-1}; ^1H NMR ($CDCl_3$) δ: 3.97 (s, 3H); 5.22 (s, 2H); 7.01–7.42 (m, 9H); 7.88 (s, 1H); 7.98 (s, 1H); 7.99 (s, 1H); 8.30 (bs, 1H); 10.93 (bs, 1H). ES-MS: (MH^+) 533.1. Anal. Calcd. for $C_{25}H_{19}N_{10}OF_3$ (MW 532.48): C, 56.39; H, 3.60; N, 26.30. Found: C, 56.53; H, 3.62; N, 26.48.

General procedure for acylation of amino group at the 5 position (5–7). Amino compound **3** (206 mg, 0.5 mmol) was dissolved in freshly distilled dioxane (15 ml) and the appropriate acyl chloride (1 mmol) and triethylamine (1 mmol, 140 μL) were added. The mixture was refluxed under argon for 18 hours. Then the solvent was removed under reduced pressure and the residue was dissolved in EtOAc (30 ml) and washed twice with water (15 ml). The organic phase was dried on anhydrous Na_2SO_4 and concentrated under reduced pressure. The residue was purified by flash chromatography (EtOAc-light petroleum 8:2) to afford the desired compounds (**5–7**).

N-{8-Methyl-2-[1-(3-trifluoromethyl-benzyl)-1H-pyrazol-4-yl]-8H-pyrazolo[4,3-e][1,2,4] triazolo[1,5-c]pyrimidin-5-yl}-benzamide (**5**): Yield 85%, pale yellow solid; mp 115°C (EtOAc-light petroleum); IR (KBr): 3240–2995, 1685, 1635, 1570, 1525 cm-1; ^{1}H NMR ($CDCl_3$) δ: 3.96 (s, 3H); 5.22 (s, 2H); 7.08–7.55 (m, 9H); 7.85 (s, 1H); 7.94 (s, 1H); 7.97 (s, 1H); 9.41 (bs, 1H). ES-MS: (MH^+) 518.2. Anal. Calcd. for $C_{25}H_{18}N_9OF_3$ (MW 517.47): C, 58.03; H, 3.51; N, 24.36. Found: C, 57.92; H, 3.44; N, 24.18.

N-{8-Methyl-2-[1-(3-trifluoromethyl-benzyl)-1H-pyrazol-4-yl]-8H-pyrazolo[4,3-e][1,2,4] triazolo[1,5-c]pyrimidin-5-yl}-phenyl-acetamide (**6**): Yield 85%, white solid; mp 190°C (EtOAc-light petroleum); IR (KBr): 3240–2990, 1675, 1605, 1580, 1525 cm-1; ^{1}H NMR ($CDCl_3$) δ: 3.96 (s, 3H); 4.27 (s, 2H); 5.20 (s, 2H); 7.03–7.37 (m, 9H); 7.82 (s, 1H); 7.94 (s, 1H); 7.97 (s, 1H); 8.82 (bs, 1H). ES-MS: (MH^+) 518.2. Anal. Calcd. for $C_{26}H_{20}N_9OF_3$ (MW 531.49): C, 58.76; H, 3.79; N, 23.72. Found: C, 58.93; H, 3.65; N, 23.88.

2-(4-Methoxy-phenyl)-N-{8-Methyl-2-[1-(3-trifluoromethyl-benzyl)-1H-pyrazol-4-yl]-8H-pyrazolo[4,3-e] [1,2,4]triazolo[1,5-c]pyrimidin-5-yl}-phenyl-acetamide (**7**): Yield 77%, yellow solid; mp 178°C (EtOAc-light petroleum); IR (KBr): 3245–2975, 1680, 1615, 1570, 1515 cm-1; ^{1}H NMR ($CDCl_3$) δ: 3.97 (s, 3H); 4.18 (s, 3H); 4.25 (s, 2H); 5.21 (s, 2H); 7.03–7.37 (m, 6H); 7.57 (d, 2H, J = 9); 7.83 (s, 1H); 7.96 (s, 1H); 7.98 (s, 1H); 8.78 (bs, 1H). ES-MS: (MH^+) 562.2. Anal. Calcd. for $C_{27}H_{22}N_9O_2F_3$ (MW 561.52): C, 57.75; H, 3.95; N, 22.45. Found: C, 57.53; H, 3.86; N, 22.33.

Biology

All pharmacological methods followed the procedures as described earlier. [33–36] In brief, membranes for radioligand binding were prepared from CHO cells stably transfected with human AR subtypes in a two-step procedure. In a first low-speed step (1,000 x g) cell fragments and nuclei were removed. The crude membrane fraction was sedimented from the supernatant at 100,000 x g. The membrane pellet was resuspended in the buffer used for the respective binding experiments (50 mM Tris/HCl buffer pH 7.4 for hA_1 and hA_{2A} AR; 50 mM Tris/HCl, 10 mM $MgCl_2$, 1 mM EDTA, pH 8.25 for hA_3 AR), frozen in liquid nitrogen and stored at -80°C. For the measurement of adenylyl cyclase activity only one high speed centrifugation of the homogenate was used. The resulting crude membrane pellet was resuspended in 50 mM Tris/HCl, pH 7.4 and immediately used for the cyclase assay.

For radioligand binding at human A_1 ARs 1 nM [^{3}H]CCPA was used (K_D = 0.61 nM), whereas 10 nM [^{3}H]NECA were used for A_{2A} (K_D = 20.1 nM). The high-affinity agonist [^{3}H] HEMADO (K_D = 1.1 nM) was used for A_3 AR binding at a concentration of 1 nM. Non specific binding of [^{3}H]CCPA was determined in the presence of 1 mM theophylline, in the case of [^{3}H]NECA and [^{3}H]HEMADO, 100 μM R-PIA was used. K_i-values from competition experiments were calculated with the program SCTFIT. [33–35]

Radioligand binding at human A_{2B} ARs is problematic as no high-affinity radioligand is commercially available for this subtype. Therefore, inhibition of NECA-stimulated adenylyl cyclase activity (stimulation with 5 μM of NECA, EC_{50} = 2.4 μM) was determined as a measurement of affinity of compounds. The procedure was carried out as described previously with minor modifications. [33–35] Membranes were incubated with about 150,000 cpm of [α-^{32}P] ATP for 20 min in the incubation mixture as described without EDTA and NaCl. [33–35]

Molecular modeling

The models for human A_1, A_{2A}, A_{2B} and A_3 ARs were retrieved from the Adenosiland platform (http://mms.dsfarm.unipd.it/Adenosiland) [36], selecting the crystallographic structure of hA_{2A} AR, in complex with the high affinity antagonist ZM241385 (PDB access code: 4EIY;

resolution 1.8 Å), as template for homology modelling. [37] The numbering of the amino acids follows the arbitrary scheme by Ballesteros and Weinstein: each amino acid identifier starts with the helix number, followed by the position relative to a reference residue among the most conserved amino acids in that helix, to which the number 50 is arbitrarily assigned. [38]

Ligand conformations were built using the MOE-builder tool implemented in the MOE suite [39] and were subjected to a MMFF94x energy minimization until the rmsd conjugate gradient was <0.05 kcal mol^{-1} $Å^{-1}$. All antagonists were docked into the hypothetical TM binding site of the hA_3 AR model derived from the centre of mass of the ZM241385 inhibitor. The workflow of the molecular docking approach used in the present work has been previously reported. [40] Molecular docking study was performed employing the docking tool of the GOLD Suite v5.2.1. [41] For each compound, 25 independent docking runs were performed and searching was conducted within a user-specified docking sphere with the Genetic Algorithm protocol and the GoldScore scoring function. The resulting docking complexes (ligand and side-chain residues within 4.5 Å) were subjected to a MMFF94x energy minimization until the rms conjugate gradient was <1 kcal mol^{-1} $Å^{-1}$.

Analyses of docking poses and quantitative analysis for nonbonded intermolecular interactions (H-bonds, hydrophobic, electrostatic) were calculated and visualized using MOE suite. [39] To estimate the electrostatic contributions, atomic charges for the ligands were calculated with MOPAC-2012 [42] and the PM3/ESP methodology, whereas partial charges for the protein amino acids were computed with the AMBER99 force field. The validation of the proposed docking protocol has been previously published. [43] Physicochemical and ADME properties of references and newly synthesized compounds were calculated with StarDropTM, version 6.0. [44]

Results and Discussion

Chemistry

Compounds **3–7** were prepared following the general synthetic strategy summarized in Fig 3. They were synthesized according to a well-known procedure for the synthesis of the PTPs, previously reported. [45–47]

Reaction of the N^2-methyl-4-cyano-5-amino pyrazole **8** with the hydrazide derivative **10** (prepared from the corresponding ester **9** [22] by reaction with hydrazine monohydrate in absolute ethanol at reflux for three days) in diphenyl ether at 260°C led to the aminotriazole **11**, which was in turn converted, without any further purification, into the final compound **3** by reaction with cyanamide in the presence of *p*-toluen sulfonic acid. Amido derivatives **5–7** were obtained by reaction of the amino compound **3** with the appropriate acyl halide in dioxane at reflux in the presence of triethylamine, while the ureido derivative **4** was obtained by reaction of the amino compound **3** with phenyl isocyanate in dioxane at reflux (Fig 3).

Biological activity

Newly synthesized compounds (**3–7**) were tested at the human A_1, A_{2A}, A_{2B} and A_3 ARs expressed in CHO (Chinese Hamster Ovary) cells. [^{3}H]CCPA ([^{3}H]2-Chloro-N^6-cyclopentyladenosine) (hA_1 AR), [^{3}H]NECA ([^{3}H]5'-*N*-ethylcarboxamidoadenosine) (hA_{2A} AR) and [^{3}H]HEMADO ([^{3}H]2-(1-Hexynyl)-*N*-methyladenosine) (hA_3 ARs) were used as radioligands in binding assays. Inhibition of NECA-stimulated adenylyl cyclase activity in CHO cells expressing hA_{2B} receptors was determined as a measurement of affinity of compounds at the hA_{2B} AR (Fig 4). [33–35]

As clearly depicted in Fig 4, surprisingly all novel CVT-like compounds do not show appreciable activity at the hA_{2B} AR. On the contrary they have shown an unexpected high affinity,

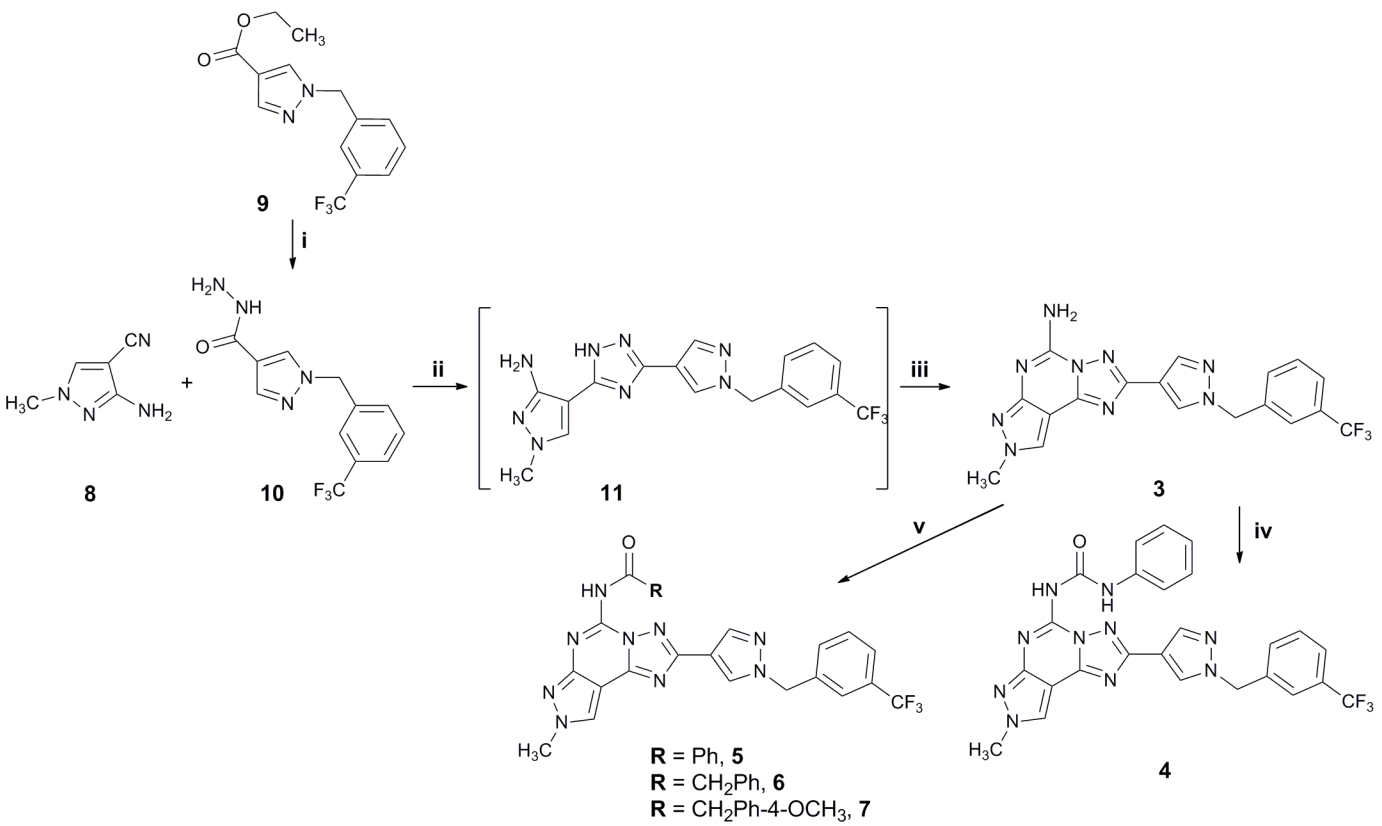

Fig 3. Synthesis of desired compounds 3–7. *Reagents*: **i**: $NH_2NH_2{\cdot}H_2O$, EtOH, reflux, 3 days; **ii**: Ph_2O, 260°C, 2.5 h; **iii**: NH_2CN, pTsOH, 160°C, 4 h; **iv**: PhNCO, dioxane, reflux; **v**: RCOCl, Et_3N, dioxane, reflux.

doi:10.1371/journal.pone.0143504.g003

with some in the nanomolar range, towards the hA_3 AR subtype. In S1 Fig representative competition curves for the hA_3 selective agonist [^{3}H]HEMADO (total binding) from single experiments for compounds **6** and **4**, respectively, are reported. The affinity at the hA_3 AR seems to be more related to the substitution at the N5 position than to the substituent present at the C2 position. In fact, the N5-unsubstituted derivative **3**, proved to be almost inactive at all four ARs, while, the introduction of a substituent at the N5 position (**4**,**7**) induced a recovery of affinity at the hA_3 AR with good levels of selectivity versus the other receptor subtypes. In particular, the introduction of an arylcarbamoyl moiety, which has been demonstrated optimal substituent for the hA_3 AR, [29–32,45–48] led to compound **4**, which shows a K_i value of 46.7 nM with a 50–70 fold selectivity versus the other receptor subtypes. The most potent compound of this series (**6**) is the derivative bearing a phenylacetyl moiety at the N5 position which shows a K_i value of 11.1 nM and high selectivity (hA_1/hA_3 and hA_{2A}/hA_3 >9090; hA_{2B}/hA_3 >909) over the other receptor subtypes. Introduction of a methoxy group on the *para* position of phenyl ring (**7**) leads to a reduction of affinity of about 5 fold (hA_3 AR K_i = 53.0 nM) with a consequent reduction of selectivity, while the replacement of phenylacetyl group with a benzoyl moiety (**5**) considerably reduces both affinity and selectivity at the hA_3 AR.

Regarding the C2 position, in a previous work it has been demonstrated that the substitution of the furyl ring at the C2 position of the PTP scaffold with a phenyl moiety gives derivatives which maintained high affinity at the hA_3 AR and showed improved selectivity at this AR subtype. [48] Moreover, with this work we have demonstrated that at the hA_3 AR bigger substituents than five or six-membered aromatic rings, such as the long chain of 1-benzyl-1*H*-

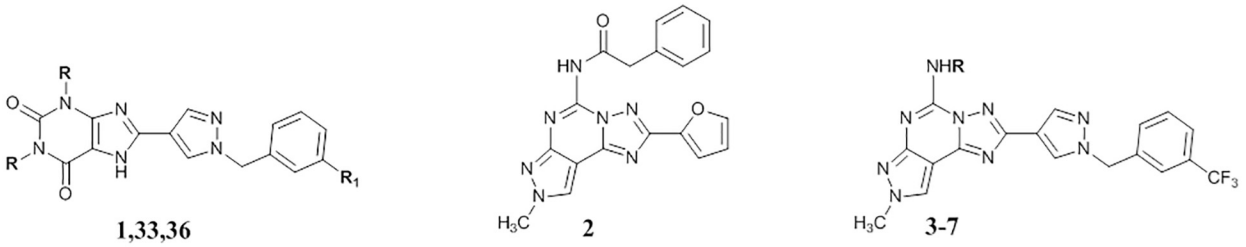

1,33,36 2 3-7

Compd	R	R_1	hA_1 AR (K_i nM)[a]	hA_{2A} AR (K_i nM)[b]	hA_{2B} AR (K_i nM)[c]	hA_3 AR (K_i nM)[d]
1[e]	CH_3	CF_3	990	690	1	1,000
2[f]	-	-	702	423	165	0.81
3	H	-	703 (573-863)	8,280 (6,240-11,000)	> 10,000	2,360 (1,490-3,750)
4	CONHPh	-	3,890 (1,870-8,110)	2,460 (1,850-3,270)	> 10,000	46.7 (39.2-55.7)
5	COPh	-	25,500 (20,200-32,200)	> 100,000	> 10,000	138 (108-175)
6	$COCH_2Ph$	-	> 100,000	> 100,000	> 10,000	11.0 (5.92-20.4)
7	$COCH_2Ph$-4-OCH_3	-	4,390 (3,720-5,190)	20,500 (17,400-24,300)	> 10,000	53.0 (33.5-83.8)
33[e]	$CH_2CH_2CH_3$	CF_3	170	230	14	56
36[e]	$CH_2CH_2CH_3$	F	170	400	14	150

Fig 4. Structures and binding profile of reference (1,2,33,36) and synthesized compounds (3–7). [a]Displacement of specific [^{3}H]-CCPA binding at hA_1 ARs expressed in CHO cells, (n = 3–6). [b]Displacement of specific [^{3}H]-NECA binding at hA_{2A} ARs expressed in CHO cells. [c]K_i values of the inhibition of NECA-stimulated adenylyl cyclase activity in CHO cells expressing hA_{2B} ARs. [d]Displacement of specific [^{3}H]-HEMADO binding at hA_3 ARs expressed in CHO cells. Data are expressed as geometric means, with 95% confidence limits. [e]data from ref. [22]. [f]data from ref. [32].

doi:10.1371/journal.pone.0143504.g004

pyrazole, are also tolerated. Obviously, this short series of compounds does not allow us to outline a structure activity relationship (SAR) analysis. In addition, the obtained results are consistent with the well-known SAR of PTP derivatives at the hA_3AR, that is: at the N5 position a substitution on the amino group is preferred and, in particular, phenylacetamido moieties are better than benzamido moieties; whereas, at the C2 position, the substitution of the furyl ring enhances selectivity versus the other receptor subtypes. [29–32,45–48] It is worth to remember that although no A_3 AR antagonist has still reached clinical trials, there are several pharmacological evidences that suggest their potential use for the treatment of asthma, chronic obstructive pulmonary disease (COPD), neurodegenerative diseases, stroke, glaucoma and cancer. [6] Consequently there is an ongoing interest in the development of novel potent and selective antagonists for the A_3 AR subtype.

Computational studies

To better rationalize these unexpected experimental results, a molecular docking study on the four hAR subtypes was performed. The workflow of the molecular docking approach used in the present work has been previously reported. [40,49] First of all, the role of the 1-(3-trifluoromethyl-benzyl)-1*H*-pyrazole-4-yl moiety in receptor recognition has been investigated starting from the analysis of the hypothetical binding mode of CTV 6975 (**1**) and two other structurally similar analogues **36** and **33** [22] against all four AR subtypes (Fig 5A). In particular, compound **36** differs in the 1,3-disubstitution of the xanthine core, where the methyl groups of

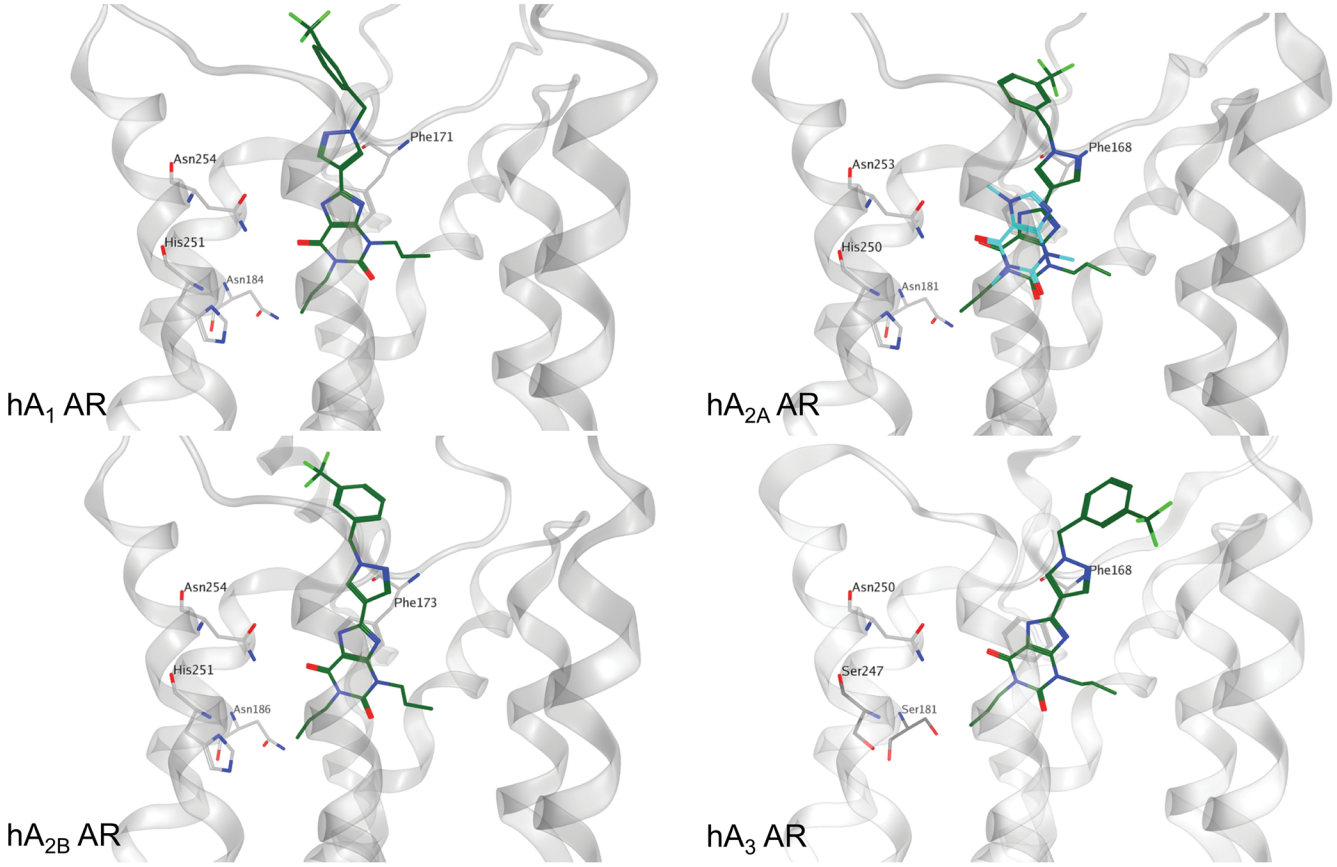

Fig 5. Binding mode of xanthine-based compounds at the four AR subtypes. Compound **36**, in dark green, was selected as reference to show the proposed binding mode at the four AR subtypes. The crystallographic coordinates of caffeine, in magenta, bound to hA_{2A} AR are reported superimposed to the binding mode of compound **36**. The xanthine core of compound **36** is oriented in a similar manner to the crystallographic data. Residues particularly important in the binding are reported as light grey sticks.

doi:10.1371/journal.pone.0143504.g005

CVT 6975 (**1**) are replaced by two propyl groups. Compound **33** shares the same substituents on the xanthine core with **36** with the trifluoromethyl group being replaced by a fluorine atom. Both compounds retain a notable affinity for the hA_{2B} AR (K_i = 14 nM) but a lower selectivity towards the other subtypes (**36**: hA_1 AR K_i = 170 nM; hA_{2A} AR K_i = 400 nM; hA_3 AR K_i = 150 nM, **33:** hA_1 AR K_i = 170 nM; hA_{2A} AR K_i = 230 nM; hA_3 AR K_i = 56 nM). [22]

Molecular docking results suggest for the three CVT analogues (**1**, **36, 33**) an univocal binding mode into the putative orthosteric pocket of the hA_{2B} AR with the xanthine core faced to the key residue Asn254 (6.55) and sided by Phe173 (EL2), Val250 (6.51) and Ile276 (7.39) (Fig 5B). The 1-benzyl-1*H*-pyrazole moiety whether substituted with trifluoromethyl or fluorine atom interacts with Met272 (7.35) and with residues located in EL2, namely Leu172-Glu174. As an example, the hypothetical binding mode of compound **36** at the hA_{2B} AR is reported in Fig 5B. Interestingly, the docking results of compound **36** at the hA_1, hA_{2A} and hA_3 ARs confirm a similar recognition pathway to that observed for the A_{2B} AR (Fig 5B). In particular, the xanthine core is positioned closely to that observed for two other xanthinic ligands, caffeine and XAC, in their crystallographic bound state at the hA_{2A} AR (PDB codes 3RFM and 3REY, respectively). [50] Moreover, molecular docking results suggest a crucial role of the 1-benzyl-1*H*-pyrazole moiety in increasing the binding affinity against all the receptor subtypes, while the nature of the

1,3-disubstitution at the xanthine core seems to play a role in determining the ligand selectivity profile. In fact, the presence of larger substituents in 1,3 positions, such as propyl groups, seems to be well tolerated at the hA_1, hA_{2A} and hA_3 ARs while at the hA_{2B} AR the 1,3-dimethyl substitution seems to guarantee the best shape complementarity in the orthosteric binding pocket.

Secondly, all newly synthesized analogues were subjected to the same docking protocol. In particular, at the hA_3 AR all compounds **4–7** showed an appreciable receptor complementarity even if two distinct plausible binding modes are detected (hereafter named A and B) analyzing all docking poses. In the binding mode A, the 1-benzyl-1*H*-pyrazole moiety is placed similarly to the CVT-like compounds previously described, with these specific interacting residues: Gln167 (EL2), Leu264 (7.35), Tyr265 (7.36). The substituent at the N5 position is inserted in an accessory pocket defined by Ser181 (5.42), Leu246 (6.51) and Ser247 (6.52). This pocket is located deeper in the TM bundle, under the Asn250 (6.51), and it is delimited by TM3 and TM5 and by Trp243 (6.48). Interestingly, this accessory pocket is probably the most relevant structural difference among the hypothetical binding sites of the AR subtypes. In particular, the Ser247 (6.52) in the hA_3 AR is not conserved in the other subtypes, replaced by an histidine in the other subtypes. This mutation significantly perturbs the shape and the of the hA_3 AR orthosteric binding pocket compared to those of all the other subtypes. More interestingly, this histidine has been reported to participate in both agonist and antagonist binding to the hA_{2A} AR by mutagenesis studies. [51,52] Also Ser181 (5.42) is a peculiarity of the hA_3 AR being replaced by conserved asparagine in the other AR subtypes.

However, in the hypothetical binding mode A the Asn250 (6.55) residue is not directly involved in the interaction with the compounds (**4**–**7**), although a water-mediated interaction could not be excluded. As an instance of binding mode A the pose of most potent analogue (**6**) is shown in Fig 6A, while the superposition of the receptor complex for **36** and **6** is reported in S4 Fig.

In the binding mode B, the position of the substituent at the C2 and N5 positions is inverted, while the orientations of the PTP core and of the methyl at N8 position are retained in the same region occupied in the binding mode A (Fig 6B and S4B Fig). The two distinct poses show similar interactions networks as demonstrated by comparing the Interaction Energy (IE) plots where the per-residue electrostatic and hydrophobic contributions are calculated (S4C Fig). Even a more quantitative comparison of the IE contributions for the most important residues reveals similar profile (Fig 6C). On the contrary, all analogues when docked into hA_1, hA_{2A} and hA_{2B} ARs did not show a stabilized binding pose comparable to those observed for the hA_3 AR. In particular compounds **4–7**, that are characterized by large substituents in both C2 and N5 positions, seem not to be able to occupy the accessory pocked that we have previously described characterizing the orthosteric binding site of the hA_3 AR. Also in this case, the analysis of the Interaction Energy (IE) plots supports the hypothesis of the complementary lacking when compounds **4–7** interact with hA_1, hA_{2A} and hA_{2B} ARs. Again, the most relevant difference can ascribed to the missing interaction with the residues delimiting the accessory cavity, as shown in S5 Fig.

The physicochemical and ADME (absorption, distribution, metabolism, and excretion) properties of the newly synthesized compounds (**3–7**) were calculated *in silico* and compared to those calculated for CVT-like derivatives and reference hA_3 AR antagonists recently reviewed by Borea *et al.* (S1 Table). [53] The PTP scaffold in comparison to the xanthine core shows a deterioration of the pharmacokinetic (PK) profile. In particular, the partition coefficient cLogP (4.49 and 2.87 for compound **6** and CVT 6975 (**1**), respectively) and the solubility are affected. Nevertheless, compound **6** and CVT 6975 (**1**) present similar ADME properties. The limitations in the pharmacokinetic profile is a common issue for the selective hA_3 AR antagonists already reported in literature. With only few exceptions, the gain in selectivity over the other human ARs subtypes is associated with a PK profile deterioration.

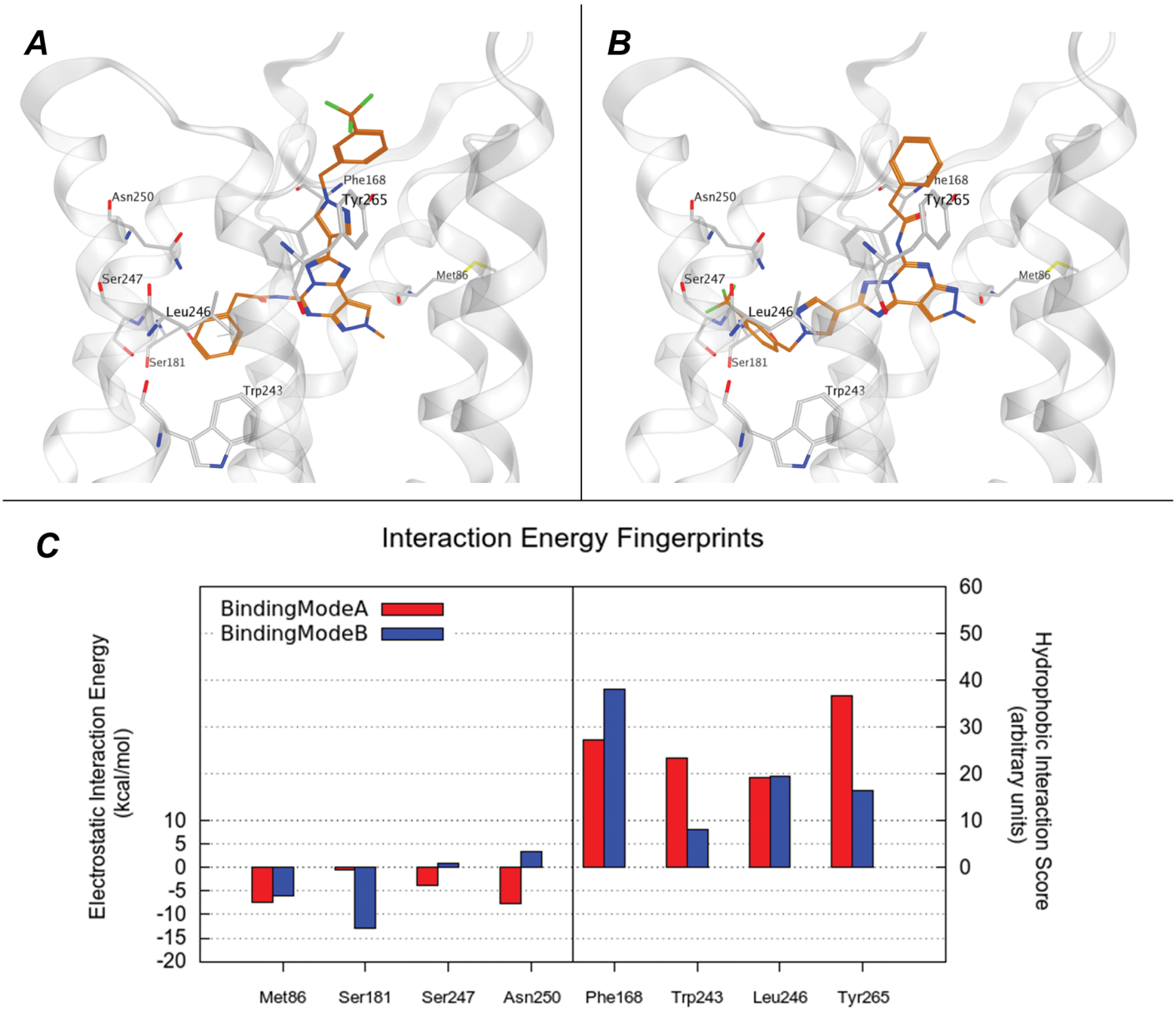

Fig 6. Binding mode of compound 6 at the hA_3 AR. (A) (B) Hypothetical binding mode A and B of newly synthetized compounds to hA_3 AR. The most potent derivative, **6**, was selected as example and is represented as orange stick. Subsets of hA_3 AR residues, involved in the binding, are coloured in light grey. (C) The electrostatic and hydrophobic contributes to interaction energy calculated for the residue mostly involved in the binding are reported compound **6** in the conformation reported in panel A (in red) and B (in blue). Electrostatic energy values are expressed in kcal mol^{-1}, whereas hydrophobic scores are expressed in arbitrary hydrophobic units.

doi:10.1371/journal.pone.0143504.g006

Conclusions

We have presented a novel series of pyrazolo[4,3-*e*][1,2,4]triazolo[1,5-*c*]pyrimidines bearing a 1-(3-trifluoromethyl-benzyl)1*H*-pyrazol-4-yl moiety at the C2 position in order to explore the effect on affinity and selectivity profiles at the four ARs. In particular, the 1-(3-trifluoromethyl-benzyl)1*H*-pyrazol-4-yl group when attached at the 8 position of xanthine derivatives, such as CVT-6975 (**1**), is known to confer high affinity for the hA_{2B} AR. Curiously, the synthesized

compounds were inactive at the hA_{2B} AR but demonstrated activity as potent and selective antagonist of the hA_3 AR. A molecular docking study was performed in order to rationalize the influence of a 1-(3-trifluoromethyl-benzyl)-1*H*-pyrazole branch. We observed that only the hA_3 AR has the topological features to accommodate this new series in agreement with experimental data. Interestingly, the ability to host such a big moiety can be ascribed to an accessory binding pocket present in the hA_3 AR, which is formed by specific unconserved residues. Two possible binding modes were proposed in which the substituents in C2 and N5 are reciprocally inverted. Further studies will be needed to validate which one is predominant or if they may co-exist. Although derivatives more potent at the hA_3 AR, and with a better drug-like properties than compound **6,** have been already reported in literature, our derivative shows high selectivity for hA_3 AR over the other ARs subtypes (S1 Table), which is comparable to other selective antagonists already reported. [53] More interestingly, the high affinity obtained by introducing long chains, such as a benzyl-1*H*-pyrazole, at the C2 position, opens to new possibilities in the development of new derivatives bearing PTP or PTP-derived simplified scaffolds. In addition, in the binding mode A, the chain at the C2 position is directed to the solvent exposed area of the hA_3 AR binding pocket, suggesting a new anchoring point for further derivatization (e.g. with fluorophore for detection purposes).

Supporting Information

S1 Fig. Competition of compounds 6 and 4 for A_3 receptor binding. Both compounds show high affinity binding to hA_3 ARs as shown by competition for the A_3 selective agonist [^{3}H] HEMADO. Representative curves (total binding) from single experiments with K_i values of 17 and 39 nM for compounds **6** and **4**, respectively, are reported.
(PDF)

S2 Fig. Competition of compound 3 for A_1 receptor binding. Compound **3** shows in a radioligand competition assay with the A_1 selective radioligand [^{3}H]CCPA a K_i value of 764 nM. The curve shows total binding to hA_1 ARs from a representative single experiment.
(PDF)

S3 Fig. Competition of compound 3 for A_{2A} receptor binding. Compound **3** shows in a radioligand competition assay with the nonselective radioligand [^{3}H]NECA a K_i value of 6820 nM. The curve shows total binding to hA_{2A} ARs from a representative single experiment.
(PDF)

S4 Fig. Hypothetical binding modes of compound 6 superimposed to compound 36 at the hA_3 AR and electrostatic and hydrophobic contributions maps for compound 6. The hypothetical binding modes (A and B respectively indicated) of compound **6** are reported superposed to the coordinates of compound **36** to reveal the similarity in the accommodation of the common 1-(3-Trifluoromethyl-benzyl)-1H-pyrazole residue. The coordinates of compound **36** in B are obtained from a secondary docking solution. (C) Per residue electrostatic interaction energy map and per residue hydrophobic interaction score map. The maps are calculated for a selected pose of compound **6** inside the hA_3 AR binding site. Electrostatic energy values are expressed in kcal mol–1, whereas hydrophobic scores are expressed in arbitrary hydrophobic units.
(TIF)

S5 Fig. Comparison of the contribution to the docking score of the key residue for the binding of compound 6 to hA_3 AR according molecular docking studies. The contributes to electrostatic and hydrophobic energy interactions for hA_1, hA_{2A}, hA_{2B} and hA_3 ARs are reported

in panels A, B, C and D respectively. In panel D, the profiles of the two predominant binding modes for hA_3 AR, A (red) and B (blue), are showed. In Panel E the location of residues Met86, Ser181, Ser247 and Asn250 (in cyan) and Phe168, Trp243, Leu246 and Tyr265 (in green) in the A_3 AR and the corresponding residues in the others AR subtypes is indicated by the ball representation of alpha Carbon atoms.
(TIF)

S1 Table. Selectivity profile and predicted physicochemical and ADME properties of references and newly synthesized compounds (3–7).
(DOCX)

Acknowledgments

S.M. is very grateful to Chemical Computing Group for the scientific and technical partnership. S.M. participates in the European COST Action CM1207 (GLISTEN).

Author Contributions

Conceived and designed the experiments: SF K-NK AC SM GS. Performed the experiments: SF SR MS SK. Analyzed the data: SF MS AC SK BC. Contributed reagents/materials/analysis tools: GS SM K-NK. Wrote the paper: SF MS BC GS.

References

1. Chen JF, Eltzsching HK, Fredholm BB. Adenosine receptors as drug targets: what are the challenges? Nat Rev Drug Discov. 2013; 12:265–286. doi: 10.1038/nrd3955 PMID: 23535933
2. Fredholm BB, IJzerman AP, Jacobson KA, Klotz KN, Linden J. International Union of Pharmacology. XXV. Nomenclature and classification of adenosine receptors. Pharm Rev. 2011; 53:527–552.
3. Fredholm BB. Adenosine receptors as drug targets. Exp Cell Res. 2010; 316:1284–1288. doi: 10.1016/j.yexcr.2010.02.004 PMID: 20153317
4. Muller CE, Jacobson KA. Recent developments in adenosine receptor ligands and their potential as novel drugs. Biochim Biophys Acta. 2011; 1808:1290–1308. doi: 10.1016/j.bbamem.2010.12.017 PMID: 21185259
5. Fredholm BB, IJzerman AP, Jacobson KA, Linden J, Muller CE. International Union of Basic and Clinical Pharmacology. LXXXI. Nomenclature and classification of adenosine receptors: an update. Pharm Rev. 2011; 63:1–34. doi: 10.1124/pr.110.003285 PMID: 21303899
6. Cheong SL, Federico S, Venkatesan G, Mandel AL, Shao YM, Moro S, et al. The A3 adenosine receptor as multifaceted therapeutic target: pharmacology, medicinal chemistry, and in silico approaches. Med Res Rev. 2013; 2:235–335.
7. Kalla RV, Zablocki J. Progress in the discovery of selective, high affinity A2B adenosine receptor antagonists as clinical candidates. Purinergic Signal. 2009; 5:21–29. doi: 10.1007/s11302-008-9119-x PMID: 18568423
8. Baraldi PG, Tabrizi MA, Fruttarolo F, Romagnoli R, Preti D. Recent improvements in the development of A2B adenosine receptor agonists. Purinergic Signal. 2009; 5: 3–19. doi: 10.1007/s11302-009-9140-8 PMID: 19184536
9. Aherne CM, Kewley EM.The resurgence of A_{2B} adenosine receptor signaling. Biochim Biophys Acta. 2011; 1808:1329–1339. doi: 10.1016/j.bbamem.2010.05.016 PMID: 20546702
10. Feoktistov I, Biaggioni I. Adenosine A2B receptors evoke interleukin-8 secretion in human mast cells. An enprofylline-sensitive mechanism with implications for asthma. J Clin Investig. 1995; 96:1979–1986. PMID: 7560091
11. Ryzhov S, Goldstein AE, Matafonov A, Zeng D, Biaggioni I, Feoktistov I. Adenosine-activated mast cells induce IgE synthesis by B lymphocytes: an A_{2B}-mediated process involving Th2 cytokines IL-4 and IL-13 with implications for asthma. J Immunol. 2004; 172:7726–7733. PMID: 15187156
12. Zhong H, Wu Y, Belardinelli L, Zeng D. A_{2B} adenosine receptors induce IL-19 from bronchial epithelial cells, resulting in TNF-alpha increase. Am J Respir Cell Mol Biol. 2006; 35:587–592. PMID: 16778150

13. Zhong H, Belardinelli L, Maa T, Feoktistov I, Biaggioni I, Zeng D. A_{2B} adenosine receptors increase cytokine release by bronchial smooth muscle cells. Am J Respir Cell Mol Biol. 2004; 30:118–125. PMID: 12855406

14. Zhong H, Belardinelli L, Maa T, Zeng D. Synergy between A_{2B} adenosine receptors and hypoxia in activating human lung fibroblasts. Am J Respir Cell Mol Biol. 2005; 32:2–8. PMID: 15472138

15. Colgan SP, Fennimore B, Ehrentraut SF. Adenosine and gastrointestinal inflammation. J Mol Med. 2013; 91:157–164. doi: 10.1007/s00109-012-0990-0 PMID: 23296303

16. Headrick JP, Ashton KJ, Rose'Meyer RB, Peart JN. Cardiovascular adenosine receptors: expression, actions and interactions. Pharmacol Therapeut. 2013; 140: 92–111.

17. Eltzschig HK, Bonney SK, Eckle T. Attenuating myocardial ischemia by targeting A_{2B} adenosine receptors. Trends Mol Med. 2013; 19:345–354. doi: 10.1016/j.molmed.2013.02.005 PMID: 23540714

18. Feoktistov I, Biaggioni I. Role of adenosine A_{2B} receptors in inflammation. Adv Pharmacol. 2011; 61:115–144. doi: 10.1016/B978-0-12-385526-8.00005-9 PMID: 21586358

19. Kong T, Westerman KA, Faigle M, Eltzschig HK, Colgan SP. HIF-dependent induction of adenosine A_{2B} receptor in hypoxia. FASEB J. 2006; 20:2242–2250. PMID: 17077301

20. Zhang Y, Dai Y, Wen J, Zhang W, Grenz A, Sun H, et al. Detrimental effects of adenosine signaling in sickle cell disease. Nat Med. 2011; 17:79–86. doi: 10.1038/nm.2280 PMID: 21170046

21. Kalla RV, Zablocki J. Progress in the discovery of selective, high affinity A2B adenosine receptor antagonists as clinical candidates. Purinergic Signal. 2009; 5:21–29. doi: 10.1007/s11302-008-9119-x PMID: 18568423

22. Kalla RV, Elzein E, Perry T, Li X, Palle V, Varkhedkar V, et al. Novel 1,3-disubstituted 8-(1-benzyl-1H-pyrazol-4-yl) xanthines: high affinity and selective A2B adenosine receptor antagonists. J Med Chem. 2006; 49:3682–3692. PMID: 16759111

23. Harada H, Asano O, Hoshino Y, Yoshikawa S, Matsukura M, Kabasawa Y, et al. 2-Alkynyl-8-aryl-9-methyladenines as novel adenosine receptor antagonists: their synthesis and structure-activity relationships toward hepatic glucose production induced via agonism of the A_{2B} receptor. J Med Chem. 2001; 44:170–179. PMID: 11170626

24. deZwart M, Vollinga RC, Beukers MW, Sleegers DF, von Frijtag Drabbe Kunzel JK, de Groote M, et al. Potent antagonists for the human adenosine A_{2B} receptor. Derivatives of the triazolotriazine adenosine receptor antagonist ZM241385 with high affinity. Drug Dev Res. 1999; 48:95–103.

25. Webb TR, Lvovskiy D, Kim SA, Ji XD, Melman N, Linden J, Jacobson KA. Quinazolines as adenosine receptor antagonists: SAR and selectivity for A_{2B} receptors. Bioorg Med Chem. 2003; 11:77–85. PMID: 12467710

26. Taliani S, Pugliesi I, Barresi E, Simorini F, Salerno S, La Motta C, et al. 3-aryl-[1,2,4]triazino[4,3-a]benzimidazol-4(10H)-one: a novel template for the design of highly selective A2B adenosine receptor antagonists. J Med Chem. 2012; 55:1490–1499. doi: 10.1021/jm201177b PMID: 22257095

27. Vidal B, Nueda A, Esteve C, Domenech T, Benito S, Reinoso RF, et al. Discovery and characterization of 4'-(2-furyl)-N-pyridin-3-yl-4,5'-bipyrimidin-2'-amine (LAS38096), a potent, selective, and efficacious A2B adenosine receptor antagonist. J Med Chem. 2007; 50:2732–2736. PMID: 17469811

28. Eastwood P, Esteve C, González J, Fonquerna S, Aiguadé J, Carranco I, et al. Discovery of LAS101057: A Potent, Selective, and Orally Efficacious A_{2B} Adenosine Receptor Antagonist. ACS Med Chem Lett. 2010; 2:213–218. doi: 10.1021/ml100249e PMID: 24900298

29. Pastorin G, Da Ros T, Spalluto S, Deflorian F, Moro S, Cacciari B, et al. Pyrazolo[4,3-*e*]-1,2,4-triazolo [1,5-*c*]pyrimidine derivatives as adenosine receptor antagonists. Influence of the N5 substituent on the affinity at the human A_3 and A_{2B} adenosine receptor subtypes: a molecular modeling investigation. J Med Chem. 2003; 46:4287–4296. PMID: 13678407

30. Baraldi PG, Cacciari B, Romagnoli R, Klotz KN, Spalluto G, Varani K, et al. Pyrazolo[4,3-e]1,2,4-triazolo[1,5-c]pyrimidine derivatives as adenosine receptor ligands: A starting point for searching A_{2B} adenosine receptor antagonists. Drug Develop Res. 2001; 53:225–235.

31. Baraldi PG, Cacciari B, Romagnoli R, Borea PA, Varani K, Pastorin G, et al. Pyrazolo-triazolo-pyrimidine derivatives as adenosine receptor antagonists: a possible template for adenosine receptor subtypes? Curr Pharm Design. 2002; 8:2299–2332.

32. Michielan L, Bolcato C, Federico S, Cacciari B, Bacilieri M, Klotz KN, et al. Combining selectivity and affinity predictions using an integrated Support Vector Machine (SVM) approach: An alternative tool to discriminate between the human adenosine A2A and A3 receptor pyrazolo-triazolo-pyrimidine antagonists binding sites. Bioorg Med Chem. 2009; 17:5259–5274. doi: 10.1016/j.bmc.2009.05.038 PMID: 19501513

33. Klotz KN, Hessling J, Hegler J, Owman C, Kull B, Fredholm BB, et al. Comparative pharmacology of human adenosine receptor subtypes—characterization of stably transfected receptors in CHO cells. Naunyn-Schmiedeberg's Arch Pharmacol. 1998; 357:1–9.

34. De Lean A, Hancock AA, Lefkowitz RJ. Validation and statistical analysis of a computer modeling method for quantitative analysis of radioligand binding data for mixtures of pharmacological receptor subtypes. Mol Pharmacol. 1982; 21:5–16. PMID: 6982395

35. Klotz KN, Cristalli G, Grifantini M, Vittori S, Lohse MJ. Photoaffinity labeling of A_1-adenosine receptors. J Biol Chem. 1985; 260:14659–14664. PMID: 2997218

36. Floris M, Sabbadin D, Medda R, Bulfone A, Moro S. Adenosiland: walking through adenosine receptors landscape. Eur J Med Chem. 2012; 58:248–257. doi: 10.1016/j.ejmech.2012.10.022 PMID: 23127988

37. Liu W, Chun E, Thompson AA, Chubukov P, Xu F, Katritch V, et al. Structural basis for allosteric regulation of GPCRs by sodium ions. Science. 2012; 337:232–236. doi: 10.1126/science.1219218 PMID: 22798613

38. Ballesteros JA, Weinstein H. Integrated methods for the construction of three-dimensional models and computational probing of structure-function relations in G protein-coupled receptors. In: Sealfon SC, editors. Methods in Neurosciences. Volume 25. San Diego, CA: Academic Press; 1995. pp. 366–428.

39. MOE (Molecular Operating Environment), version 2014.09; Chemical Computing Group Inc., 1010 Sherbooke St. West, Suite #910, Montreal, Quebec, Canada, 2014.

40. Ciancetta A, Cuzzolin A, Moro S. Alternative quality assessment strategy to compare performances of GPCR-ligand docking protocols: the human adenosine A_{2A} receptor as a case study. J Chem Inf Model. 2014; 54:2243–2254. doi: 10.1021/ci5002857 PMID: 25046649

41. GOLD suite, version 5.2.1; Cambridge Crystallographic Data Centre, Cambridge.

42. Stewart, J. J. P.MOPAC 7; Fujitsu Limited, Tokyo, Japan, 1993.

43. Cheong SL, Dolzhenko AV, Paoletta S, Lee EP, Kachler S, Federico S, et al. Does the combination of optimal substitutions at the C^2-, N^5- and N^8-positions of the pyrazolo-triazolo-pyrimidine scaffold guarantee selective modulation of the human A_3 adenosine receptors? Bioorg Med Chem. 2011; 19:6120–6134. doi: 10.1016/j.bmc.2011.08.026 PMID: 21908194

44. Stardrop™, version 6.0; Optibrium Ltd: 7221 Cambridge Research Park, Beach Drive, Cambridge CB25 9TL, UK.

45. Moro S, Braiuca P, Deflorian F, Ferrari C, Pastorin G, Cacciari B, et al. Combined target-based and ligand-based drug design approach as a tool to define a novel 3D-pharmacophore model of human A_3 adenosine receptor antagonists: pyrazolo[4,3-*e*]1,2,4-triazolo[1,5-*c*]pyrimidine derivatives as a key study. J Med Chem. 2005; 48:152–162. PMID: 15634009

46. Gatta F, Del Giudice MR, Borioni A, Borea PA, Dionisotti S, Ongini E. Synthesis of imidazo[1,2-*c*]pyrazolo[4,3-*e*]pyrimidines, pyrazolo[4,3-*e*]1,2,4-triazolo[1,5-*c*]pyrimidines and triazolo[5,1-*i*]purines: new potent A_2 adenosine receptor antagonists. antagonists. Eur J Med Chem. 1993, 28:569–577.

47. Baraldi PG, Cacciari B, Romagnoli R, Spalluto G, Moro S, Klotz KN, et al. Pyrazolo[4,3-*e*]1,2,4-triazolo [1,5-*c*]pyrimidine derivatives as highly potent and selective human A_3 adenosine receptor antagonists: influence of the chain at the N(8) pyrazole nitrogen. J Med Chem. 2000; 43:4768–4780. PMID: 11123985

48. Cheong SL, Dolzhenko A, Kachler S, Paoletta S, Federico S, Cacciari B, et al. The significance of 2-furyl ring substitution with a 2-(para-substituted) aryl group in a new series of pyrazolo-triazolo-pyrimidines as potent and highly selective hA_3 adenosine receptors antagonists: new insights into structure-affinity relationship and receptor-antagonist recognition. J Med Chem. 2010; 53:3361–3375. doi: 10.1021/jm100049f PMID: 20307065

49. Cuzzolin A, Sturlese M, Malvacio I, Ciancetta A, Moro S. DockBench: an integrated informatic platform bridging the gap between the robust validation of docking protocols and virtual screening simulations. molecules. 2015; 20:9977–9993. doi: 10.3390/molecules20069977 PMID: 26035098

50. Dore AS, Robertson N, Errey JC, Ng I, Hollenstein K, Tehan B, et al. Structure of the adenosine A2A receptor in complex with ZM241385 and the xanthines XAC and caffeine. Structure. 2011; 19:1283–1293. doi: 10.1016/j.str.2011.06.014 PMID: 21885291

51. Gao ZG, Chen A, Barak D, Kim SK, Muller CE, Jacobson KA. Identification by site-directed mutagenesis of residues involved in ligand recognition and activation of the human A3 adenosine receptor. J Biol Chem. 2002; 277: 19056–19063. PMID: 11891221

52. Jiang Q, Lee BX, Glashofer M, van Rhee AM, Jacobson KA. Mutagenesis reveals structure-activity parallels between human A2A adenosine receptors and biogenic amine G protein-coupled receptors. J Med Chem. 1997; 40:2588–2595. PMID: 9258366

53. Borea PA, Varani K, Vincenzi F, Baraldi PG, Tabrizi MA, Merighi S, Gessi S. The A3 adenosine receptor: history and perspectives. Pharmacol Rev. 2015; 67:74–102. doi: 10.1124/pr.113.008540 PMID: 25387804